Optical deformation-potential scattering of holes in multiple quantum well structures

K. Reimann,* R. A. Kaindl,† M. Woerner
Max-Born-Institut für Nichtlineare Optik und Kurzzeitspektroskopie, Max-Born-Straße 2A, 12489 Berlin, Germany
(Received 1 August 2001; published 14 December 2001)

The lifetime of excited states in intersubband transitions of holes in nonionic semiconductors, e.g., in $Si_{1-x}Ge_x$, is determined predominantly by optical deformation-potential scattering. We present a theory for the calculation of the scattering rates. It includes strain and confinement, the hole-hole Coulomb interaction in Hartree-Fock approximation, and the different possible optical phonon branches. As a consequence of the symmetry of the optical deformation tensor the scattering rate between subbands of different types (e.g., from a heavy-hole subband to a light-hole or split-off subband) is considerably higher than between subbands of the same type. Numerical results are given for $Si_{1-x}Ge_x/Si$ quantum wells with various Ge concentrations and well widths. We find that the scattering rates decrease both with increasing Ge concentration in the wells and with increasing well width. From this one can derive guidelines how to achieve lifetimes long enough to allow the operation of a silicon-based quantum cascade laser.,,

DOI: 10.1103/PhysRevB.65.045302 PACS number(s): 73.21.Fg, 72.10.Di, 78.47.+p

I. INTRODUCTION

In semiconductor quantum wells, the two-dimensional confinement leads to the emergence of subbands within the conduction and valence bands, which results in a multitude of novel electronic and optical properties. An important new relaxation process is intersubband scattering: carriers promoted into a higher subband via thermal, optical or electronic excitation are scattered into lower subbands by phonon emission or by interacting with other charge carriers.

For electrons, numerous studies, both experimental and theoretical, have revealed a detailed picture.[1–5] A subband separation larger than the energy of a LO phonon results in the emission of polar LO phonons within typically one picosecond. For smaller subband spacings, the rate is significantly reduced as mainly electron-electron scattering remains. Scattering via the deformation potential plays no marked role in the conduction band for reasons of symmetry.

In contrast, only scarce information is available about the dynamics of holes. Here the scattering is determined by other processes and deformation potential interaction can exhibit very high rates in the valence band since it can couple the *p*-wave components of the cell-periodic wave functions. Recently, an experiment[6] has been carried out that has determined the relaxation of holes in SiGe/Si quantum wells after optical intersubband excitation of heavy-hole states, finding rapid relaxation within ≈ 250 fs. As is well known, the valence band in tetrahedral semiconductors is considerably more complicated than the conduction band. Some theoretical calculations for intersubband scattering of holes are reported,[7–12] but they fail to take into account the important interplay between the symmetries of the hole wave functions and that of the matrix elements correctly. A comprehensive treatment which includes these effects is essential here, but has not been carried out up to now.

Aside from physical insights, an understanding of these fundamental interactions is important also for the accurate engineering of semiconductor devices, where single component plasmas as in quantum cascade structures[13] are of specific current interest. Silicon is nowadays the most widely utilized semiconductor, as nearly all commercial electronics is based on this material. Light-emitting devices, however, form an important exception due to the indirect band gap of Si. Nevertheless, it is still a goal of research to integrate the semiconductor laser onto a silicon microelectronics chip. Here, the use of intersubband transitions in $Si_{1-x}Ge_x/Si$ quantum wells as the lasing transition might constitute a viable, novel approach.[12] In contrast to quantum cascade lasers based on[13] $In_xGa_{1-x}As/Al_yIn_{1-y}As$ or[14] $GaAs/Al_xGa_{1-x}As$, which use intersubband transitions of electrons, the $Si_{1-x}Ge_x/Si$ system uses intersubband transitions of holes. While first measurements show electroluminescence[15,16] in such a structure, lasing has not yet been observed.

In this paper, we provide a detailed theory of the scattering of holes inside valence subbands of semiconductor quantum wells. The calculation takes into account hole-phonon scattering via the deformation potential, which is the dominant process in the nonionic group-IV semiconductors. We include the effects of symmetry, strain, and confinement, as well as the hole-hole Coulomb interaction, and the different optical phonon branches that occur in this system. Results of these calculations are reported for $Si_{1-x}Ge_x/Si$ heterostructures in a wide range of parameters. As the relaxation determines the important lifetime of the upper laser level in a quantum cascade structure, we provide guidelines how to maximize this lifetime.

The present paper is organized as follows. In Sec. II we give an overview over our band structure calculations, since the calculation of scattering matrix elements necessitates the wave functions of initial and final states. The calculations are based on the eight-band $\mathbf{k}\cdot\mathbf{p}$ approximation, which yields reasonably accurate results[17] in the range of wave vectors near $k=0$ that is accessible by optical phonon scattering, with acceptable computation times. Many-particle effects are treated in the full Hartree-Fock approximation. The subsequent section (Sec. III) provides a description of the deformation potential interaction of holes with optical phonons, which is the central issue of this paper. The effects of symmetry and phonon modes are included and discussed explicitly. Then, in Sec. IV we give our results for $Si_{1-x}Ge_x/Si$ multiple quantum well structures with different well widths

and Ge concentrations. Finally, we conclude in Sec. V with guidelines for achieving long lifetimes in *p*-type quantum cascade structures based on this system.

II. BAND STRUCTURE CALCULATIONS

We perform the calculation of the electronic band structure of heterostructures in the eight-band $\mathbf{k}\cdot\mathbf{p}$ approximation. First we consider the bulk band structure of the constituent materials including spin-orbit coupling and strain. In Sec. II B the wave functions and energies for the heterostructures are obtained from a plane-wave basis. The carrier-carrier interaction is included in the full Hartree-Fock approximation (Sec. II C).

A. Bulk Hamiltonian

Within the eight-band $\mathbf{k}\cdot\mathbf{p}$ approximation, bulk wave functions for the wave vector $\mathbf{k}$ are given as linear combinations

$$\psi_{\mathbf{k}} = e^{i\mathbf{k}\cdot\mathbf{r}} \sum_{v=1}^{8} b_{v\mathbf{k}} |v\rangle \tag{1}$$

of the following eight basis functions $|v\rangle$ (xyz representation):[18]

$$s\uparrow, p_x\uparrow, p_y\uparrow, p_z\uparrow, s\downarrow, p_x\downarrow, p_y\downarrow, p_z\downarrow. \tag{2}$$

The direction of the arrow indicates the z component of the electron spin, and s, p_x, etc., give the symmetry of the cell-periodic parts of the wave function. Very often another set of basis functions is chosen, namely, one which is diagonal in the total angular momentum J [heavy-hole ($J=3/2$, $J_z=\pm 3/2$), light-hole ($J=3/2$, $J_z=\pm 1/2$), and split-off ($J=1/2$, $J_z=\pm 1/2$) bands].[19,20] Whereas this second choice gives a simpler form for the spin-orbit coupling, all other parts (e.g., the $\mathbf{k}\cdot\mathbf{p}$ interaction and the deformation) of the total Hamiltonian get more complicated.

The Hamiltonian $H_{\mathbf{k}}$ without carrier-carrier interaction, but including the effect of strain, is given in Ref. 18. It depends on the following parameters: the energy gap E_g, the valence-band offset Δ_{VB}, the mass parameters A, L, M, and N, which describe interactions with additional bands not included explicitly, the momentum matrix element P between s and p states, the spin-orbit coupling Δ_{SO}, the difference of the hydrostatic deformation potentials[21,22] of conduction and valence bands $a_c - a_v$, and the tetragonal deformation potential b. In general there is an additional contribution due to the trigonal deformation potential, but this is zero for our case of pseudomorphic growth on a (001) surface.

Without the tetragonal deformation, at $k=0$ the Hamiltonian leads to the typical band structure of cubic semiconductors, namely a twofold degenerate conduction band and two valence bands, one fourfold and the other twofold degenerate. For $k\neq 0$, the fourfold band splits into heavy- and light-hole bands. With the tetragonal deformation, the fourfold degeneracy is lifted already at $k=0$, resulting in three twofold degenerate valence bands. Additionally, the tetragonal deformation introduces a mixing between light-hole and split-off bands. Because of this, valence bands can only be designated either as heavy-hole (HH) or as light-hole–split-off (LHSO). Further mixing occurs for $k\neq 0$, so that a band with 100% heavy-hole character at $k=0$ gets light-hole and split-off contributions for $k\neq 0$ (and vice versa). We will designate bands according to their character at $k=0$.

B. Heterostructures

There are two possibilities for calculating the energies and wave functions in a heterostructure in the envelope-function approach:[23–26] One of these is to solve the Hamiltonian independently in each layer. The allowed states are then found from boundary conditions at the interfaces between the layers. This method is well suited if one considers exclusively conduction band electrons without any coupling to the valence band. In contrast, the technique becomes very difficult to carry out for an eight-component wave function. Moreover, including the full electron-electron interactions (see below) prevents an analytical solution in this case.

Because of these problems we choose a second possibility,[19] namely, to solve the Hamiltonian for the total structure with spatially varying parameters along the growth direction, taken as z [$E_g = E_g(z)$, $A = A(z)$, etc.]. In the growth direction we choose periodic boundary conditions [$\psi(z+l) = \exp(ik_z l)\psi(z)$] with l equal to the period length of the structure, i.e., to the sum of well and barrier widths. In this way we calculate a three-dimensional crystal with the (rather large) lattice constant l in z direction. This has the advantage that one can use the same formalism both for superlattices and for uncoupled quantum wells simply by changing the barrier width. As in any crystal, the resulting wave functions can be classified according to their band (or subband) index N and by their wave vector $\mathbf{k}$ in the first Brillouin zone. This implies especially that $|k_z| \leqslant \pi/l$.

Functions which automatically fulfill the boundary conditions given above and which form a complete set are plane waves $e^{in\mathbf{K}\cdot\mathbf{r}}$ (n is an integer) with the length of $\mathbf{K}$ equal to $2\pi/l$ and its direction parallel to the growth direction (z in our case). Thus, a wave function belonging to the state N and the wave vector $\mathbf{k}$ can be written as

$$\psi_{N\mathbf{k}}(\mathbf{r}) = \frac{1}{\sqrt{V}} e^{i\mathbf{k}\cdot\mathbf{r}} \sum_{n,v} g_{N,n,v,\mathbf{k}} e^{in\mathbf{K}\cdot\mathbf{r}} |v\rangle. \tag{3}$$

The summation index n runs from $-\infty$ to ∞ (for numerical calculations one uses instead of ∞ a suitably chosen $n_{\max}$), and the index v over the states given in Eq. (2). V is the normalization volume.

The complex coefficients $g_{N,n,v,\mathbf{k}}$ and the energy $E_{N\mathbf{k}}$ are found from calculating the matrix elements of $H_{\mathbf{k}}$ and determining then the eigenvalues and eigenvectors. For the structures we have studied, it is sufficient to choose $n_{\max}$ between 12 and 22. This results in matrix sizes $(16n_{\max}+8)$ between 200 and 360, which are easily tractable on a typical PC.

C. Carrier-carrier interaction

The above Hamiltonian is suitable only in the absence of free carriers. Since we consider, however, structures with

rather high carrier densities (e.g., by modulation doping), the interaction between the carriers needs to be included. It consists of the direct (H^d) and the exchange (H^e) Coulomb interaction. In the Hartree-Fock approximation, these interactions induce additional couplings between states with band indices M and M' (or energy shifts for $M=M'$), which are given by

$$H^d_{M,M',\mathbf{k}}=\sum_{N,\mathbf{q}} f_{N\mathbf{q}}U_{(M\mathbf{k})(M'\mathbf{k})(N\mathbf{q})(N\mathbf{q})}+U_{\text{doping}},$$

$$H^e_{M,M',\mathbf{k}}=-\sum_{N,\mathbf{q}\neq\mathbf{k}} f_{N\mathbf{q}}U_{(M\mathbf{k})(N\mathbf{q})(N\mathbf{q})(M'\mathbf{k})}, \tag{4}$$

with

$$U_{(N_1\mathbf{k}_1)(N_2\mathbf{k}_2)(N_3\mathbf{k}_3)(N_4\mathbf{k}_4)}=-q_e^2\int\int\frac{\psi^*_{N_1\mathbf{k}_1}(\mathbf{r})\psi_{N_2\mathbf{k}_2}(\mathbf{r})\psi^*_{N_3\mathbf{k}_3}(\mathbf{r}')\psi_{N_4\mathbf{k}_4}(\mathbf{r}')}{4\pi\epsilon_0\epsilon_r|\mathbf{r}-\mathbf{r}'|}dVdV'$$

$$=-\frac{q_e^2}{V}\sum_{\substack{n,v,p\\m,u}}\frac{g^*_{N_1,m,u,\mathbf{k}_1}g_{N_2,m+p,u,\mathbf{k}_2}g^*_{N_3,n,v,\mathbf{k}_3}g_{N_4,n-p,v,\mathbf{k}_4}}{\epsilon_0\epsilon_r|\mathbf{k}_1-\mathbf{k}_2+p\mathbf{K}|^2}\delta_{\mathbf{k}_1-\mathbf{k}_2+\mathbf{k}_3-\mathbf{k}_4,0}. \tag{5}$$

For $\mathbf{k}_1=\mathbf{k}_2$ the term with $p=0$ is omitted. In these equations q_e is the elementary charge, ϵ_0 is the vacuum dielectric constant (SI units), ϵ_r is a background dielectric constant caused by the screening from all other electrons, and $f_{N\mathbf{q}}$ is the occupation of the state with wave vector $\mathbf{q}$ and index N. In thermal equilibrium at the temperature T, $f_{N\mathbf{q}}$ is the Fermi distribution for holes

$$f_{N\mathbf{q}}=\frac{1}{\exp\left(\dfrac{-E_{N\mathbf{q}}-\mu}{k_BT}\right)+1}. \tag{6}$$

The chemical potential μ has to be chosen so that the total number of carriers is equal to the number of carriers present by doping or by interband excitation. In doped material there is an extra term U_{doping} due to the potential of the ionized acceptors/donors. Because of the dependence of H^d and H^e on the carrier distribution, the resulting band structure becomes temperature dependent even without an explicit temperature dependence of the band structure parameters.

The direct Coulomb term H^d is determined by the carrier density. It can be transformed into an electrostatic potential, so that its action on all states is about the same. This is in contrast to the exchange part H^e, which mainly acts on states with the same symmetry as the occupied states. Thus, if only subband 1 is occupied, the effect of H^e is strongest for subband 1 and rapidly decreases for higher subbands. Therefore, since the calculation of H^e is quite time consuming, we restrict M and M' to the three lowest-energy subbands. Especially, we do not consider Auger terms, i.e., contributions with M equal to an electron and M' equal to a hole subband (or vice versa). The reason for this is that apart from their small values such contributions go beyond the one-electron model used here, since they allow generation of electron-hole pairs.

Because of the considerable computational effort needed to evaluate H^e from Eq. (4), there exist a large number of approximations.[27] Most of these construct a carrier-density dependent electrostatic potential that shifts the energy levels in the same way as the exchange interaction. While this approach typically gives satisfactory ground state energies, the excited states are much less accurate, since an electrostatic potential has the same influence on both ground and excited states, whereas the exchange interaction acts mainly on the ground state, as already mentioned above. A second shortcoming of all density-functional approximations is that they are only applicable to a limited range of carrier densities. Because of these problems we employ here the exact expression for the exchange, Eq. (4).

Since the expressions for H^d and H^e [Eq. (4)] include the eigenvectors and [via Eq. (6)] the energies for all occupied states, first one solves $H_{\mathbf{k}}$ without carrier-carrier interaction for a sufficient number of points in $\mathbf{k}$ space. From Eq. (4) one finds that to calculate H^d and H^e one has to include all points in $\mathbf{k}$ space which have non-negligible occupation. The distribution spreads out for increasing temperature, and thus the volume in $\mathbf{k}$ space (and with it the numerical effort) increases considerably with temperature. To determine how fine the spacing Δk between adjacent $\mathbf{k}$ points has to be to achieve a reasonable accuracy, we have compared the results for the free-electron case, which can be solved analytically, with the results of the summation in Eq. (4). It turns out that already at $T=0$ it is necessary to calculate the exchange energy H^e (H^d converges much faster) at more than 3600 points (plus the symmetry-equivalent points) in $\mathbf{k}$ space to achieve an accuracy of better than 0.5 meV. Since, however, the error is to a very good approximation linear in Δk (we use the same spacing in x, y, and z direction), i.e., $H^e(\Delta k)=H^e(\Delta k\rightarrow 0)+C\Delta k$ with some (unknown) constant C, $H^e(\Delta k\rightarrow 0)$ can be found with extremely high precision[28] from $H^e(\Delta k\rightarrow 0)=2H^e(\Delta k)-H^e(2\Delta k)$. With this expression only 60 points are needed for the same accuracy of 0.5 meV or, conversely, the same number of points as above now yields an accuracy of better than 2 μeV.

With these matrix elements for H^d and H^e one then solves the Schrödinger equation for the total Hamiltonian

$$H^{\text{total}}_{\mathbf{k}}=H_{\mathbf{k}}+H^d_{\mathbf{k}}+H^e_{\mathbf{k}}. \tag{7}$$

From the new solutions one then calculates improved values for H^d and H^e, solves again H^{total} and so on until convergence is reached. We use as criterion for convergence that the maximum energy deviation between two steps is less than 50 μeV. Fortunately, convergence is rather fast, so that typically just two iterations are needed.

III. DEFORMATION POTENTIAL SCATTERING

The electronic band structure is determined by the atoms in the unit cell. Accordingly, a change of atomic positions leads to changes of the band structure, the so-called deformation-potential interaction.[21] Such changes of atomic positions can occur either because of externally applied stress or because of phonons. External stress leads to a static band structure change, which has to be taken into account in calculations of strained quantum wells (see above). Phonons, on the other hand, lead to dynamic changes, which may allow intra- or interband scattering of carriers. In the harmonic approximation the phonon scattering matrix elements M_{if} are linear in the atomic displacements $\mathbf{u}$:[29,30] $M_{if} = \langle i|\mathbf{D}\cdot\mathbf{u}|f\rangle$.

In the following we will restrict ourselves to scattering by optical phonons in semiconductors with diamond structure (point group $O_h \hat{=} m3m$).[31] The high symmetry of this structure limits the number of states between which scattering is possible[32] and determines the form of the tensor $\mathbf{D}$. To decide whether scattering between the states i and f is allowed, one has to determine the symmetric part of the direct product $\Gamma_f \times \Gamma_i$ [Γ_f and Γ_i are the irreducible representations (or symmetries) of these states]. If this product contains the symmetry of the phonon involved, the scattering is allowed. Under the usual assumption that the deformation potential interaction does not couple states with different spin it is sufficient to consider the single-group representations. Since the optical phonons near the zone center have Γ_5^+ symmetry (we give the irreducible representations in the notation of Koster *et al.*[33]), intraband scattering is allowed for bands with Γ_4^+, Γ_4^-, Γ_5^+, and Γ_5^- symmetries. In particular, intraconduction-band scattering is forbidden, but intravalence-band scattering is allowed, since the uppermost valence band of diamond-type semiconductors typically has Γ_4^- symmetry. More detailed selection rules can be obtained from the tables of coupling coefficients in Ref. 33. One finds that scattering from an x-like state into an y-like state is only allowed if the elongation of the optical phonon is parallel to z.[30,34,35] All other allowed processes are obtained by permutation of x, y, and z (see Fig. 1). If one considers the angular momentum basis (the basis functions are then heavy-hole, light-hole, and split-off bands), this interaction again only couples states of different types. For example, a heavy hole is not coupled to other heavy-hole states, but to light-hole and split-off bands (see Fig. 1).

Although these selection rules are known since more than 40 years,[30] there exist a considerable number of papers[7–12] which do not use the selection rules, but simply assume that the scattering is proportional to the wave function overlap. Accordingly, they predict wrong lifetimes.

On the basis of these symmetry considerations, the optical deformation potential tensor $\mathbf{D}$ takes the following form:[36,34]

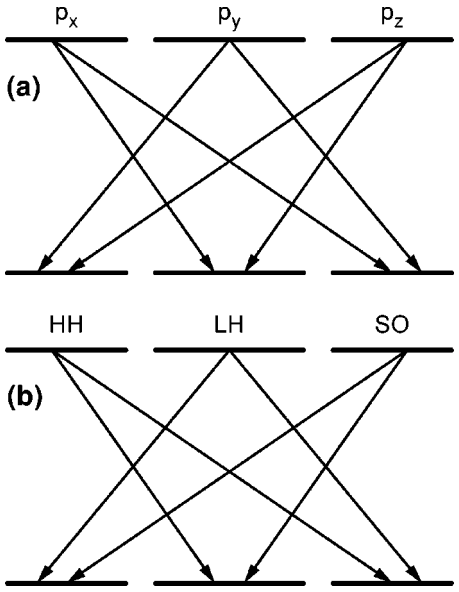

FIG. 1. Possible scattering channels by the optical deformation potential in the (a) xyz basis and in the (b) angular momentum basis.

$$\mathbf{D} = \frac{d_0}{a}\left[\begin{pmatrix} d_x & 0 \\ 0 & d_x \end{pmatrix}, \begin{pmatrix} d_y & 0 \\ 0 & d_y \end{pmatrix}, \begin{pmatrix} d_z & 0 \\ 0 & d_z \end{pmatrix}\right], \tag{8}$$

with

$$d_x = \begin{pmatrix} 0 & 0 & 0 & 0 \\ 0 & 0 & 0 & 0 \\ 0 & 0 & 0 & 1 \\ 0 & 0 & 1 & 0 \end{pmatrix}, \quad d_y = \begin{pmatrix} 0 & 0 & 0 & 0 \\ 0 & 0 & 0 & 1 \\ 0 & 0 & 0 & 0 \\ 0 & 1 & 0 & 0 \end{pmatrix},$$

$$d_z = \begin{pmatrix} 0 & 0 & 0 & 0 \\ 0 & 0 & 1 & 0 \\ 0 & 1 & 0 & 0 \\ 0 & 0 & 0 & 0 \end{pmatrix}.$$

The strength of this interaction is determined by the optical deformation potential constant d_0, which for typical semiconductors[37] is on the order of several ten eV. Unfortunately, there exist several definitions for the prefactor in Eq. (8) (for example, the prefactor d_0' in Ref. 37 is equal to $\sqrt{8/3}d_0$) and for the displacement $\mathbf{u}$. Whereas some authors[38,34] define as $\mathbf{u}$ the displacement of one of the two atoms in the primitive cell of the diamond structure, others[30] (including us) define it as the difference of the displacements of the two atoms. The advantage of the second definition is that it can be used equally well for structures where the two atoms have different masses and, accordingly, different amplitudes (this is the case not only for zinc blende, but also for the SiGe alloys considered here).

Using Fermi's Golden Rule, the total scattering rate from the initial state $\psi_{N,\mathbf{k}}$ into all other states $\psi_{N',\mathbf{k}'}$ is given by

$$W_{N,\mathbf{k}}=\frac{2\pi}{\hbar}\sum_{N',\mathbf{k}',j,\mathbf{q}}|\langle\psi_{N',\mathbf{k}'}|\mathbf{D}\cdot\mathbf{u}_j(\mathbf{q})|\psi_{N,\mathbf{k}}\rangle|^2 \times\{\delta[E_{N,\mathbf{k}}-E_{N',\mathbf{k}'}-\hbar\Omega_j(\mathbf{q})][1+n_j(\mathbf{q})] + \delta[E_{N,\mathbf{k}}-E_{N',\mathbf{k}'}+\hbar\Omega_j(\mathbf{q})]n_j(\mathbf{q})\}. \quad (9)$$

The first term in the braces corresponds to phonon emission, the second to phonon absorption. In this equation $\mathbf{u}_j(\mathbf{q})$ is the displacement of the phonon mode j with wave vector $\mathbf{q}$, energy $\hbar\Omega_j(\mathbf{q})$, and occupation $n_j(\mathbf{q})$, which is assumed to be at the thermal-equilibrium value. In the diamond structure there is no splitting between transverse and longitudinal optical phonons at $\mathbf{q}=0$, which leads to a threefold degeneracy. We will assume in the following that the energy of the optical phonon is independent of the wave vector (which is a very good approximation, since only phonons in a small part near the center of the Brillouin zone are involved), $\hbar\Omega_j(\mathbf{q})=\hbar\Omega_j$ and accordingly $n_j(\mathbf{q})=n_j$. One should note that Eq. (9) does not contain an explicit dependence on the wave vector $\mathbf{q}=\mathbf{k}'-\mathbf{k}$ of the optical phonon involved, in contrast to, e.g., polar optical scattering.

In bulk material the phonon displacement $\mathbf{u}$ in Eq. (9) is position independent. The amplitude can be found from the requirement that the total energy of the phonon is equal to $\hbar\Omega$. In a heterostructure it is more difficult to determine the phonon amplitudes, which will in general depend on position within the heterostructure. The best way would be to perform a lattice-dynamical calculation for the whole structure.[3] It turns out, however, that nearly identical scattering rates can be obtained from a much simpler model. We assume that for the phonons the heterostructure is equivalent to bulk material with the composition of the wells. The justification for this is that phonon amplitudes are only of interest in the regions where $|\psi(\mathbf{r})|^2$ has appreciable magnitude. For bound states this is just the case in the wells. Since the phonon amplitudes in the barriers do not matter, we can simply assume that these amplitudes are the same as in the wells.

From these considerations the displacement $\mathbf{u}_j(\mathbf{q})$ is given by

$$\mathbf{u}_j(\mathbf{q})=\sqrt{\alpha_j\frac{\hbar a^3}{2V\Omega_j\mu_j}}\,\hat{e}_j\exp(i\mathbf{q}\cdot\mathbf{r}), \quad (10)$$

with μ_j the reduced mass of the two atoms in the primitive unit cell, $\hat{e}_j$ a unit vector along x, y, or z, and $\mathbf{r}$ the position of the primitive unit cell. The factor α describes the phonon amplitudes for the different types of optical phonons which are possible. As an example, in a $Si_{1-x}Ge_x$ alloy optical phonons may be either Ge-Ge-like (the two atoms in the primitive unit cell are both Ge, $\mu=m_{Ge}/2$) with a phonon energy of 36 meV, Si-Ge-like (the primitive unit cell contains one Si and one Ge atom, $\mu^{-1}=m_{Ge}^{-1}+m_{Si}^{-1}$, energy 50 meV), or Si-Si-like ($\mu=m_{Si}/2$) with an energy of 60 meV.[39] Since x of all atoms are Ge atoms, x^2 of all primitive unit cells contain two Ge atoms. Thus, for Ge-Ge-like phonons $\alpha=x^2$, for Si-Ge-like phonons $\alpha=2x(1-x)$, and for Si-Si-like phonons $\alpha=(1-x)^2$.

TABLE I. Band-structure and lattice (lattice constant a and elastic constants c_{ij}) parameters used for $Si_{1-x}Ge_x$/Si quantum wells. The data for the $Si_{1-x}Ge_x$ alloy are obtained by linear interpolation between the values for Si and Ge, except for the valence band parameter M, where we use the nonlinear interpolation formula of Ref. 40. The references used are given in the last column.

	Si	Ge	Refs.
E_g (eV)	4.185	0.898	41
A	0	0	
L	0	0	
M	-4.6	-5.75	41
N	0	0	
$P^2/2m_0$ (eV)	26.8	26.8	42
Δ_{SO} (meV)	44	297	41
Δ_{VB} (meV)	0	470	43,44
a (pm)	543.10	565.79	41
c_{11} (GPa)	165.8	124.0	41
c_{12} (GPa)	63.9	41.3	41
b (eV)	-2.2	-2.4	41
a_c-a_v (eV)	-5	-12.7	42,41
ϵ_r	11.9	16.1	41,42

The phonon wave vector $\mathbf{q}$ in Eq. (10) can be written as $\mathbf{q}=\mathbf{Q}+p\mathbf{K}$, with $\mathbf{Q}$ restricted to the first Brillouin zone of the heterostructure and p an integer. The matrix element in Eq. (9) then yields the selection rule $\mathbf{Q}=\mathbf{k}'-\mathbf{k}$. From Eqs. (3), (9), and (10), the scattering rate caused by x-polarized phonons of type j is given by:

$$W_{N,\mathbf{k},j,x}=\frac{\pi\alpha_j d_0^2 a}{V\Omega_j\mu_j}\sum_{N',\mathbf{k}',p}\Big|\sum_n g^*_{N',n-p,3,\mathbf{k}'}g_{N,n,4,\mathbf{k}} + g^*_{N',n-p,4,\mathbf{k}'}g_{N,n,3,\mathbf{k}}+g^*_{N',n-p,7,\mathbf{k}'}g_{N,n,8,\mathbf{k}} + g^*_{N',n-p,8,\mathbf{k}'}g_{N,n,7,\mathbf{k}}\Big|^2[\delta(E_{N,\mathbf{k}}-E_{N',\mathbf{k}'}-\hbar\Omega_j) \times(1+n_j)+\delta(E_{N,\mathbf{k}}-E_{N',\mathbf{k}'}+\hbar\Omega_j)n_j]. \quad (11)$$

According to Eq. (8), for y polarized phonons the indices (3,4,7,8) in Eq. (11) change to (2,4,6,8) and for z polarized phonons to (2,3,6,7). Although the volume V is explicitly contained in Eq. (11), the final result does not depend on V, since the number of possible $\mathbf{k}'$ is proportional to V [to be specific, if one calculates the energies and wave functions on a three-dimensional grid in k space with a spacing of Δk, the volume is $V=(2\pi/\Delta k)^3$]. The accuracy of the numerical calculation of the scattering rate increases with decreasing Δk. The maximum $|\mathbf{k}|$ has to be chosen to include the final states after phonon scattering.

IV. RESULTS

In this section we present our results for the HH2 scattering rates in $Si_{1-x}Ge_x$/Si multiple quantum wells. For the calculation of scattering rates it is necessary to first calculate the electronic band structure. The parameters used for our band structure calculations are compiled in Table I. One

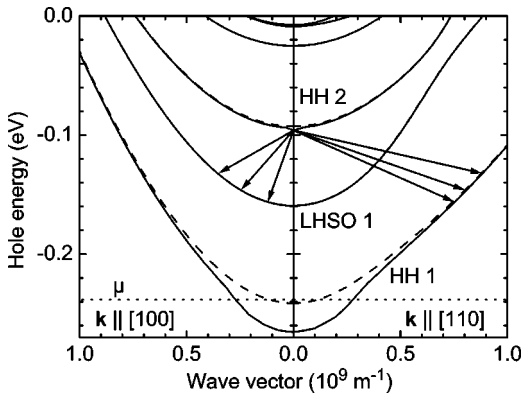

FIG. 2. Band structure of a $Si_{0.5}Ge_{0.5}/Si$ multiple quantum well structure with 4.4-nm wells and 18-nm barriers. The dashed lines give the energies without and the solid lines with exchange interaction (the chemical potential μ for the second case is shown by the dotted line). The arrows show possible scattering channels for the three types of optical phonons.

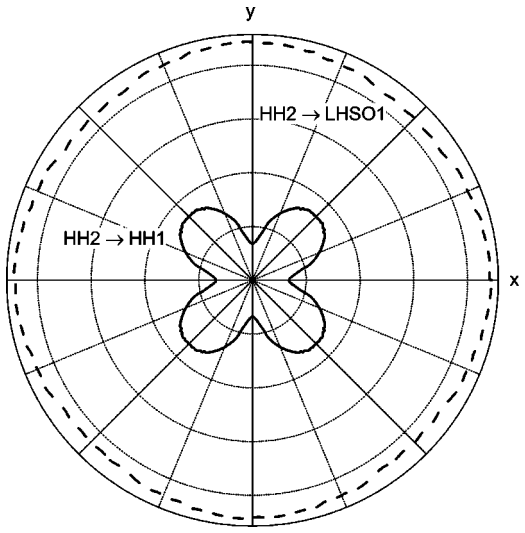

FIG. 3. Angular dependence of the scattering rate from the HH2 state at $k=0$ to the LHSO1 state (dashed line) and to the HH1 state (solid line) for the same structure as in Fig. 2.

should note that the parameters *A*, *L*, and *N* have different values for six- and eight-band $\mathbf{k}\cdot\mathbf{p}$ calculations, since in the eight-band calculation the interaction with the conduction bands is included explicitly. In the six-band calculation this interaction is incorporated into the parameters (the six-band parameter is the one usually given in data compilations[42,41]) according to[45–47]

$$X^{(6)}=X^{(8)}+\frac{P^2}{2m_0}\frac{1}{3}\left(\frac{2}{E_g}+\frac{1}{E_g+\Delta_{\mathrm{SO}}}\right) \tag{12}$$

(X is one of *A*, *L*, and *N*). It turns out that the correct electron and hole masses (including their direction dependence) are obtained for $X^{(8)}=0$ for the whole range of Ge concentrations. This means that the coupling of the valence band to other conduction bands can be neglected for these three parameters. The only parameter which is influenced by higher conduction bands is *M*. Since we do not consider explicitly these higher conduction bands (it would need a 14-band calculation to do this), *M* remains Ge-concentration dependent and thus position dependent.

As an example for a band-structure calculation according to Sec. II, we show in Fig. 2 the valence band structure, i.e., the hole energy (which is equal to minus the energy of an electron in the valence band) as a function of the in-plane wave vector $\mathbf{k}$, for $Si_{0.5}Ge_{0.5}/Si$ multiple quantum wells with 4.4-nm thick wells and 18-nm thick barriers. The carrier density per well is 1.2×10^{12} cm^{-2} from δ doping the center of the barriers. For the following we are interested in the three valence bands with the lowest hole energies, namely, HH1, LHSO1, and HH2. One can see a pronounced warping (the energy is different for different directions of $\mathbf{k}$) and an avoided crossing between LHSO1 and HH2 for $\mathbf{k}\|[110]$. Further, Fig. 2 shows the effect of the exchange interaction. One sees that the exchange interaction decreases the energy of the occupied HH1 band near $k=0$ by 17 meV. Accordingly, the energetic distance between HH2 and HH1 increases by this amount. We would like to point out that the calculation of this rather important effect necessitates the full Hartree-Fock Hamiltonian. Density-functional approximations, in contrast, will not lead to changes of the HH2-HH1 distance. The energy difference caused by the exchange interaction decreases with increasing $|\mathbf{k}|$; it extends in $\mathbf{k}$ space to about $2k_F$. In contrast, the other bands, which are unoccupied at the low temperatures we consider here (12 K), are almost unaffected by the exchange interaction.

We use the energies and eigenvectors from the band-structure calculation to determine the HH2 scattering rate. Scattering can occur either to the LHSO1 or to the HH1 band. The arrows in Fig. 2 show the possible channels for scattering out of the HH2 band with the participation of the three types of optical phonon possible in a SiGe alloy. A calculation according to Eq. (11) with $d_0=22$ eV (this corresponds to the deformation potential constant $d_0'=\sqrt{8/3}d_0=36$ eV in Ref. 37) at a temperature of 12 K yields a total scattering rate of 3.4 ps^{-1}, which corresponds to a HH2 lifetime of[48] 290 fs. This result agrees very well with the experimental result in Ref. 6 of 250 ± 100 fs.

The scattering rate from the HH2 at $k=0$ to the LHSO1 (2.6 ps^{-1}) is more than three times larger than the scattering rate to the HH1 (0.8 ps^{-1}). This is what one expects from the selection rules given in Sec. III, since HH2-HH1 scattering is forbidden at $k=k'=0$ (see Fig. 1). It becomes allowed only through the LH and SO admixtures to the HH1 state for $k'>0$. This is further illustrated in Fig. 3 by a plot of the scattering rates from HH2 at $k=0$ to LHSO1 and HH1 as a function of the direction of the wave vector $\mathbf{k}'$ of the final state. One can see that the scattering to HH1 is much larger in [110] directions than in [100] directions, whereas the scattering to LHSO1 is nearly isotropic. The reason for this is that the LHSO1 wave functions are mainly LH- and SO-like, independent of the direction of $\mathbf{k}'$. In contrast, the HH1 wave functions are mainly HH-like with only a small admixture of LH and SO. This admixture increases with increasing $|\mathbf{k}'|$,

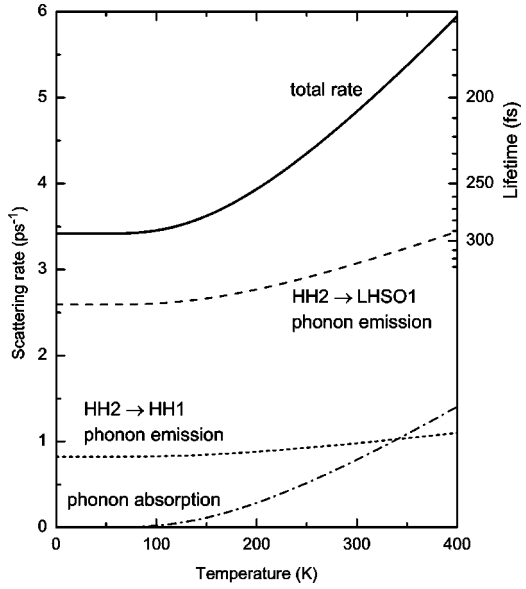

FIG. 4. Temperature dependence of the different scattering rates from the HH2 state at $k=0$ for the same structure as in Fig. 2.

since it is caused by the nondiagonal terms in the $\mathbf{k}\cdot\mathbf{p}$ Hamiltonian.[18] Because of the warping of the valence band (see Fig. 2) $|\mathbf{k}'|$ (and therefore the scattering rate) is larger for scattering into the [110] direction as compared to the [100] direction.

The temperature dependence of the scattering rates (see Fig. 4) is determined mainly by the phonon occupation numbers n_j in Eq. (11). The band structure also changes with temperature because of the temperature dependence of the band-structure parameters and the change of the exchange interaction with temperature, but this has only rather small effects on the phonon scattering rates. One sees in Fig. 4 that the scattering rates are nearly constant up to a temperature of about 150 K. For higher temperatures they increase (to a large part caused by the onset of phonon absorption processes), but because of the high phonon energies this increase is quite moderate (the lifetime at room temperature is 210 fs compared to 290 fs at 0 K).

In order to determine the dependence of HH2 scattering rates on well width and Ge concentration it is necessary to perform a band-structure calculation for each structure. Because of the computational effort involved, we do not include the exchange interaction in these calculations. As seen in Fig. 2, this means that the HH2-HH1 distance will be too small by about 17 meV (this energy difference has only a rather small well-width dependence). For a given well width the HH2 lifetimes calculated with and without exchange interaction are almost identical (for 4.4-nm well width these lifetimes differ by less than 1 fs).

In Fig. 5 we summarize the band structure calculations. Shown are the HH2 and the LHSO1 energies relative to the HH1 energy as a function of the well width for Ge concentrations of $x=0.3$, 0.5, and 0.7. The period (sum of well and barrier widths) is held constant at $l=22.4$ nm, i.e., we have nearly uncoupled quantum wells. The carrier density per well is 1.2×10^{12} cm^{-2} from δ doping the middle of the barriers.

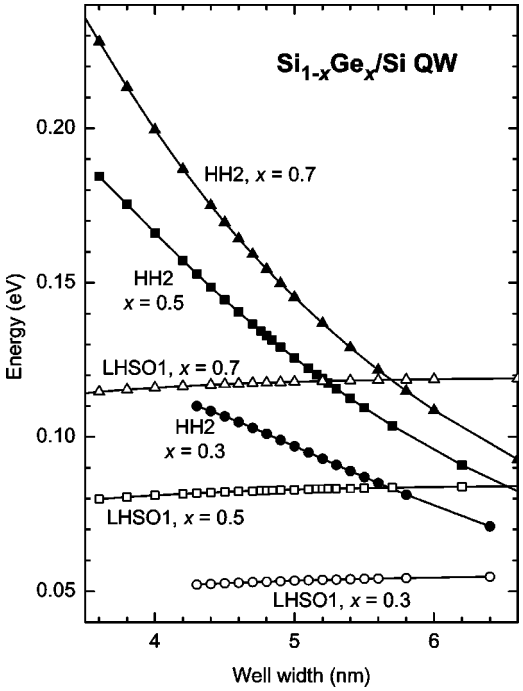

FIG. 5. Energies of the LHSO1 and the HH2 band at $k=0$ for $Si_{1-x}Ge_x$/Si multiple quantum wells for Ge concentrations of $x=0.3$, 0.5, and 0.7 as a function of well width, calculated without taking into account the exchange interaction. The HH1 band at $k=0$ is chosen as the zero of energy.

One can see from Fig. 5 that the HH2-HH1 distance strongly decreases with increasing well width as expected for a quantum well. In contrast, the energy difference between LHSO1 and HH1 is almost independent of the well width, since it is determined nearly exclusively by the built-in strain and thus by the Ge concentration x in the wells.

For a Ge concentration of $x=0.5$ we show in Fig. 6 the scattering rates from the HH2 at $k=0$ as a function of the HH2-HH1 distance, which is changed by varying the well width (upper scale). The HH2-HH1 scattering rate increases monotonically with the energetic distance, since the final states will have increasingly larger k' and thus larger LH and SO admixtures. In contrast, the HH2-LHSO1 scattering rate shows a steplike behavior. It increases when scattering by an additional type of optical phonon becomes possible. Thus the HH2 lifetime drops from 2050 fs for a well width of 5.3 nm (here no optical phonon can participate) to 290 fs for a well width of 4.5 nm (all three types of phonon can participate). For even thinner wells the HH2 lifetime stays about constant (the increase of the HH2-HH1 rate being compensated by the decrease of the HH2-LHSO1 rate).

In Fig. 7 we present the total scattering rates for $Si_{1-x}Ge_x$ quantum wells with $x=0.3$, 0.5, and 0.7. Again the steplike behavior can be observed. Comparing the rates for different values of x one finds that for all transition energies the rates decrease with increasing x. This is caused by two effects: For the HH2-LHSO1 scattering the thresholds for each type of optical phonon are reached at higher transition energies, since the LHSO1-HH1 distance increases with x (see Fig. 5), which means that the HH2-LHSO1 distance decreases. The

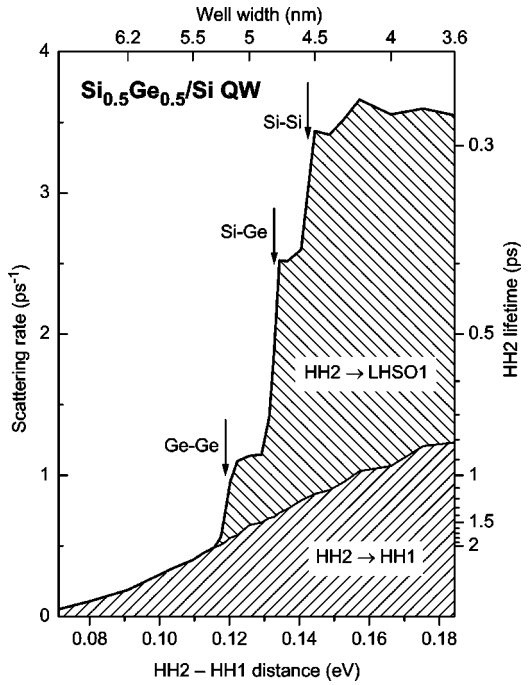

FIG. 6. Calculated scattering rates (left scale) and lifetimes (right scale) at zero temperature from the optical phonon deformation potential scattering for $Si_{0.5}Ge_{0.5}/Si$ multiple quantum wells as a function of the HH2-HH1 distance (varied by varying the well width, see upper scale). The total scattering rate is divided into the rate from HH2 to LHSO1 and into the rate from HH2 to HH1. The arrows show the thresholds for scattering by Ge-Ge, Si-Ge, and Si-Si type optical phonons.

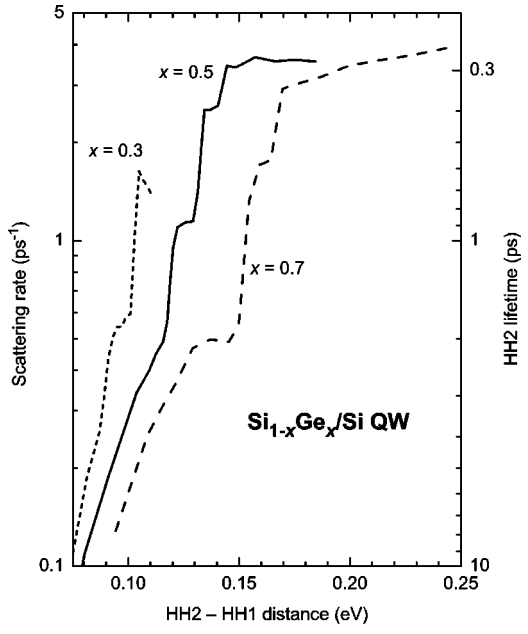

FIG. 7. Calculated total scattering rates at zero temperature for optical phonon deformation potential scattering for $Si_{1-x}Ge_x/Si$ multiple quantum wells for Ge concentrations of $x=0.3$, 0.5, and 0.7 as a function of the HH2-HH1 distance.

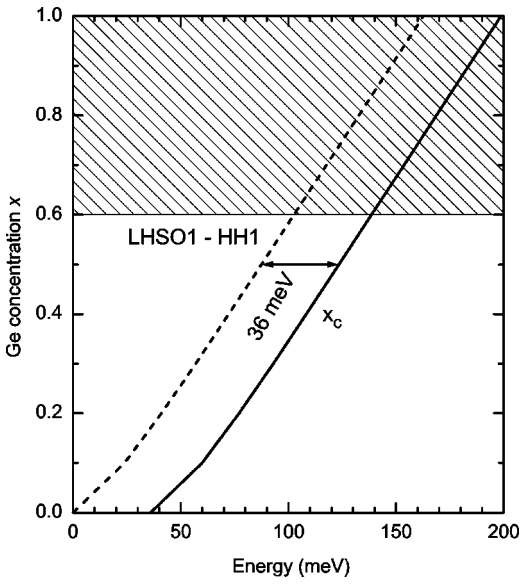

FIG. 8. Minimum Ge concentration x_c to achieve a HH2-LHSO1 difference less than the optical Ge-Ge phonon energy of 36 meV, calculated from the LHSO1-HH1 distance, as a function of the HH2-HH1 transition energy. In the shaded area ($x>0.6$) the strain makes it impossible to grow such samples.

HH2-HH1 scattering, which is determined by the LH and SO admixtures to the HH1 wave function, decreases with x since the increasing LHSO1-HH1 distance leads to smaller LH and SO admixtures.

V. CONCLUSIONS FOR SiGe-BASED QUANTUM CASCADE LASERS

For a laser it is advantageous to have a long lifetime in the upper laser level. Structures have been proposed,[12] and even luminescence (but not lasing) was observed in a recent experiment,[15,16] with HH2→HH1 as the anticipated lasing transition. Since, as we have seen, scattering into LHSO1 is much more efficient than scattering into HH1, one can achieve comparatively long lifetimes (>1 ps, which would be similar to excited state lifetimes in electron intersubband transitions) at low temperatures, if scattering into LHSO1 is not possible. This is the case if the energy difference between HH2 and LHSO1 is less than one optical phonon energy. Since the energy difference between LHSO1 and HH1 is determined mainly by the strain, it increases with the Ge concentration x in the wells (see Fig. 5). Thus, for a given HH2-HH1 distance, x has to be above a critical value x_c to achieve E_{HH2}-$E_{\mathrm{LHSO1}}<\hbar\Omega$ (see Fig. 8). For a given value of x, the transition energy depends on the well thickness. It turns out that if one uses the Ge concentration x_c from Fig. 8, the necessary quantum well thickness is approximately constant at 5 nm. Because of the rather large built-in strain, 5-nm wide quantum wells can only be grown[49,50] for Ge concentrations up to $\approx 60\%$. This limits the maximum laser photon energy to about 120 meV. One should note that the strain is responsible for the decrease of the HH2-LHSO1 distance, which eventually makes LO-phonon scattering im-

possible. Therefore schemes which reduce the strain by using, e.g., graded SiGe buffers, are going to *reduce* the lifetime. However, to be able to grow a quantum cascade structure, which consists of a large number of wells (the limit given above of 60% Ge concentration for a 5-nm well applies to a single well), one has to find a way to compensate for the strain. One possibility for this is to use barriers with the opposite sign of the strain, for example,[51,52] $Si_{1-y}C_y$.

On the other hand, the lifetimes as shown in Fig. 7 are very promising at lower energies (longer wavelengths). For the long-wavelength range both Si and Ge have the additional advantage that they do not possess infrared-active phonons, which limit the longest wavelengths to be reached with zinc blende semiconductors.

ACKNOWLEDGMENTS

We acknowledge financial support from the Deutsche Forschungsgemeinschaft.

*Electronic address: reimann@mbi-berlin.de

†Present address: Lawrence Berkeley National Lab., 1 Cyclotron Road, Berkeley, CA 94720.

[1] R. Ferreira and G. Bastard, Phys. Rev. B **40**, 1074 (1989).

[2] M. C. Tatham, J. F. Ryan, and C. T. Foxon, Phys. Rev. Lett. **63**, 1637 (1989).

[3] I. Lee, S. M. Goodnick, M. Gulia, E. Molinari, and P. Lugli, Phys. Rev. B **51**, 7046 (1995).

[4] S. Lutgen, R. A. Kaindl, M. Woerner, T. Elsaesser, A. Hase, H. Künzel, M. Gulia, D. Meglio, and P. Lugli, Phys. Rev. Lett. **77**, 3657 (1996).

[5] T. Elsaesser and M. Woerner, Phys. Rep. **321**, 253 (1999).

[6] R. A. Kaindl, M. Wurm, K. Reimann, M. Woerner, T. Elsaesser, C. Miesner, K. Brunner, and G. Abstreiter, Phys. Rev. Lett. **86**, 1122 (2001).

[7] K. Bhaumik, B. K. Ridley, and Y. Shacham-Diamand, J. Appl. Phys. **74**, 5546 (1993).

[8] Z. Xu, P. M. Fauchet, C. W. Rella, B. A. Richman, H. A. Schwettman, and G. W. Wicks, Phys. Rev. B **51**, 10 631 (1995).

[9] G. Sun, L. Friedman, and R. A. Soref, Appl. Phys. Lett. **66**, 3425 (1995).

[10] G. Sun and L. Friedman, Phys. Rev. B **53**, 3966 (1996).

[11] G. Sun, Y. Lu, L. Friedman, and R. A. Soref, Phys. Rev. B **57**, 6550 (1998).

[12] L. Friedman, R. A. Soref, and G. Sun, J. Appl. Phys. **83**, 3480 (1998).

[13] J. Faist, F. Capasso, D. L. Sivco, A. L. Hutchinson, C. Sirtori, and A. Y. Cho, Science **264**, 553 (1994).

[14] C. Sirtori, P. Kruck, S. Barbieri, P. Collot, J. Nagle, M. Beck, J. Faist, and U. Oesterle, Appl. Phys. Lett. **73**, 3486 (1998).

[15] G. Dehlinger, L. Diehl, U. Gennser, H. Sigg, J. Faist, K. Ensslin, D. Grützmacher, and E. Müller, Science **290**, 2277 (2000).

[16] H. Sigg, G. Dehlinger, L. Diehl, U. Gennser, S. Stutz, J. Faist, D. Grützmacher, K. Ensslin, and E. Müller, Physica E **11**, 240 (2001).

[17] Z. Ikonic, R. W. Kelsall, and P. Harrison, in *Proceedings of the 25th International Conference on the Physics of Semiconductors*, Osaka, 2000, edited by N. Miura and T. Ando (Springer, Berlin, 2001), p. 479.

[18] P. Enders, A. Bärwolff, M. Woerner, and D. Suisky, Phys. Rev. B **51**, 16 695 (1995).

[19] T. Fromherz, E. Koppensteiner, M. Helm, G. Bauer, J. F. Nützel, and G. Abstreiter, Phys. Rev. B **50**, 15 073 (1994).

[20] R. Oszwaldowski and G. Fishman, Physica E (Amsterdam) **4**, 11 (1999).

[21] J. Bardeen and W. Shockley, Phys. Rev. **80**, 72 (1950).

[22] G. E. Pikus and G. L. Bir, Fiz. Tverd. Tela **1**, 1642 (1959) [Sov. Phys. Solid State **1**, 1502 (1960)].

[23] G. Bastard, Phys. Rev. B **24**, 5693 (1981).

[24] G. Bastard, Phys. Rev. B **25**, 7584 (1982).

[25] M. G. Burt, J. Phys.: Condens. Matter **4**, 6651 (1992).

[26] D. J. BenDaniel and C. B. Duke, Phys. Rev. **152**, 683 (1966).

[27] W. Kohn, Rev. Mod. Phys. **71**, 1253 (1999).

[28] W. H. Press, B. P. Flannery, S. A. Teukolsky, and W. T. Vetterling, *Numerical Recipes in C*, 2nd ed. (Cambridge University Press, Cambridge, 1997),

[29] W. Harrison, Phys. Rev. **104**, 1281 (1956).

[30] G. L. Bir and G. E. Pikus, Fiz. Tverd. Tela **2**, 2287 (1960) [Sov. Phys. Solid State **2**, 2039 (1960)].

[31] All the results are also applicable to semiconductors with zincblende structure. In this case one has to make the following substitutions $\Gamma_1^+ \rightarrow \Gamma_1$, $\Gamma_4^+ \rightarrow \Gamma_4$, $\Gamma_4^- \rightarrow \Gamma_5$, $\Gamma_5^+ \rightarrow \Gamma_5$, $\Gamma_5^- \rightarrow \Gamma_4$. Additionally one has to consider the splitting between transverse and longitudinal phonons.

[32] P. Lawaetz, Phys. Rev. **166**, 763 (1968).

[33] G. F. Koster, J. O. Dimmock, R. G. Wheeler, and H. Statz, *Properties of the Thirty-Two Point Groups* (MIT Press, Cambridge, MA, 1963).

[34] M. Woerner and T. Elsaesser, Phys. Rev. B **51**, 17 490 (1995).

[35] R. Scholz, J. Appl. Phys. **77**, 3219 (1995).

[36] E. O. Kane, Phys. Rev. **178**, 1368 (1969).

[37] W. Pötz and P. Vogl, Phys. Rev. B **24**, 2025 (1981).

[38] A. Cantarero, C. Trallero-Giner, and M. Cardona, Phys. Rev. B **39**, 8388 (1989).

[39] M. I. Alonso and K. Winer, Phys. Rev. B **39**, 10 056 (1989).

[40] M. M. Rieger and P. Vogl, Phys. Rev. B **48**, 14 276 (1993).

[41] *Landolt-Börnstein – Zahlenwerte und Funktionen aus Naturwissenschaften und Technik*, edited by O. Madelung (Springer, Berlin, 1987), Vol. III/22a.

[42] *Landolt-Börnstein – Zahlenwerte und Funktionen aus Naturwissenschaften und Technik*, edited by O. Madelung (Springer, Berlin, 1982), Vol. III/17a.

[43] C. G. Van de Walle and R. M. Martin, Phys. Rev. B **34**, 5621 (1986).

[44] L. Colombo, R. Resta, and S. Baroni, Phys. Rev. B **44**, 5572 (1991).

[45] E. O. Kane, J. Phys. Chem. Solids **1**, 82 (1956).

[46] E. O. Kane, in *Semiconductors and Semimetals*, edited by R. K. Willardson and A. C. Beer (Academic Press, New York, 1966), Vol. 1, p. 75.

[47] P. Y. Yu and M. Cardona, *Fundamentals of Semiconductors* (Springer, Berlin, 1996).

[48] The slight difference to the theoretical value given in Ref. 6 (225

fs) is due to our now considering the three types of phonon, whereas in Ref. 6 we have only considered an average phonon. Further, we have now used a finer grid in k space.

[49] J. Y. Tsao, B. W. Dodson, S. T. Picraux, and D. M. Cornelison, Phys. Rev. Lett. **59**, 2455 (1987).

[50] S. C. Jain and W. Hayes, Semicond. Sci. Technol. **6**, 547 (1991).

[51] S. S. Iyer, K. Eberl, M. S. Goorsky, F. K. LeGoues, J. C. Tsang, and F. Cardone, Appl. Phys. Lett. **60**, 356 (1992).

[52] K. Brunner, K. Eberl, and W. Winter, Phys. Rev. Lett. **76**, 303 (1996).